

MHD Natural Convection in a Nanofluid-filled Enclosure with Non-uniform Heating on Both Side Walls

Imen Mejri^{1,2}, Ahmed Mahmoudi¹, Mohamed Ammar Abbassi¹
and Ahmed Omri¹

Abstract: This study examines natural convection in a square enclosure filled with a water- Al_2O_3 nanofluid and subjected to a magnetic field. The side walls of the cavity have spatially varying sinusoidal temperature distributions. The horizontal walls are adiabatic. A Lattice Boltzmann method (LBM) is applied to solve the governing equations for fluid velocity and temperature. The following parameters and related ranges are considered: Rayleigh number of the base fluid, from $\text{Ra}=10^3$ to 10^6 , Hartmann number from $\text{Ha}=0$ to 90, phase deviation ($\gamma=0, \pi/4, \pi/2, 3\pi/4$ and π) and solid volume fraction of the nanoparticles between $\phi=0$ and 6%. The results show that the heat transfer rate increases with an increase in the Rayleigh number but it decreases with an increase in the Hartmann number. For $\gamma = \pi/2$ and $\text{Ra}=10^5$ the magnetic field strengthens the effect produced by the presence of nanoparticles. For $\text{Ha}=0$, the most evident influence of nanoparticles is achieved at $\gamma = 0$ and $\pi/4$ for $\text{Ra}=10^4$ and 10^5 respectively.

Keywords: Lattice Boltzmann Method, Natural convection, nanofluid, magnetic field, Sinusoidal temperature distribution.

Nomenclature

B	Magnetic field (T)
c	Lattice speed (m/s)
c_s	Speed of sound (m/s)
c_i	Discrete particle speeds (m/s)
c_p	Specific heat at constant pressure ($\text{JKg}^{-1}\text{K}^{-1}$)
F	External forces (N)
f	Density distribution functions (kg m^{-3})

¹ UR: Unité de Recherche Matériaux, Energie et Energies Renouvelables (MEER), Faculté des Sciences de Gafsa, B.P.19, Zarroug, Gafsa, 2112, Tunisie.

² Corresponding Author. Email: im.mejri85@yahoo.fr; Tel: 00216 25345419.

f^{eq}	Equilibrium density distribution functions (kg m⁻³)
g	Internal energy distribution functions (K)
g^{eq}	Equilibrium internal energy distribution functions (K)
\vec{g}	Gravity vector (m s⁻²)
Ha	Hartmann number
k	thermal conductivity (Wm⁻¹ K⁻¹)
Ma	Mach number
n	Number of nodes
Nu	Local Nusselt number
P	Pressure (N m⁻²)
Pr	Prandtl number
Ra	Rayleigh number
T	Temperature (K)
$\mathbf{u}(u, v)$	Velocities (m/s)
$\mathbf{x}(x, y)$	Lattice coordinates (m/s)

Greek symbols

Δx	Lattice spacing (m)
Δt	Time increment (s)
τ_α	Relaxation time for temperature (s)
τ_ν	Relaxation time for flow (s)
ν	Kinematic viscosity (m² s⁻¹)
α	Thermal diffusivity (m² s⁻¹)
ρ	Fluid density (kg m⁻³)
σ	electrical conductivity (S/m)
ψ	Non-dimensional stream function
ϕ	Solid volume fraction
μ	Dynamic viscosity (N s /m²)
γ	phase deviation
θ	Non-dimensional temperature

Subscript

b	bottom
c	cold
f	fluid
h	hot
l	left

<i>m</i>	mean
<i>nf</i>	nanofluid
<i>p</i>	particle
<i>r</i>	right

1 Introduction

The problem of natural convection in square enclosures has many engineering applications such as: cooling systems of electronic components, building and thermal insulation systems, built-in-storage solar collectors, nuclear reactor systems, food storage industry and geophysical fluid mechanics and many others [Ostrach (1988); Al-Ajmi and Mosaad, (2012); Hamimid, Guellal, Amroune and Zeraibi, (2012); Moufekkik, Moussaoui, Mezrhab, Naji and Bouzidi, (2012); Choukairy and Ben-nacer, (2012); Arid, Kousksou, Jegadheeswaran, Jamil, Zeraouli, (2012); Dihmani, Amraoui, Mezrhab and Laraqi, (2012); Shemirani and Saghir, (2013); Maougal and Bessaïh, (2013); Kamath, Balaji and Venkateshan, (2013); Rtibi, Hasnaoui and Amahmid, (2013); Mahrouche, Najam, El Alami, Faraji, (2013); Rana and Thakur, (2013); Haslavsky, Miroshnichenko, Kit, and Gelfgat, (2013)]. In some practical cases such as crystal growth, metal casting, fusion reactors and geothermal energy extractions, natural convection is under the influence of a magnetic field [Moreau (1990); Ozoe and Okada (1989); Garandet et al. (1992); Venkatachalappa and Subbaraya (1993); Alchaar et al. (1995); Rudraiah et al. (1995)]. Khanafar et al. (2003) numerically investigated natural convection heat transfer in a two-dimensional vertical enclosure utilizing nanofluids. It was revealed that the heat transfer rate increases with the increase of particle fraction at any given Grashof number. Kahveci (2010) numerically studied the heat transfer enhancement of water-based nanofluids in a differentially heated, tilted enclosure for a range of inclination angles, nanoparticle volume fractions, and Rayleigh numbers. It was concluded from the results that suspended nanoparticles substantially increase the heat transfer rate and the average Nusselt number is nearly linear with the increase of solid volume fraction. However, Putra et al. (2003) conducted experiments to investigate natural convective heat transfer of aqueous CuO and Al₂O₃ nanofluids inside a cylinder. They observed a systematic and significant deterioration in natural convective heat transfer at Rayleigh numbers from 10⁶ to 10⁹. The deterioration increased with particle concentration and was more pronounced for CuO nanofluids. Wen and Ding (2005) reported that for a Rayleigh number less than 10⁶, the natural convection heat transfer rate increasingly decreases with the increase of particle fraction, particularly at low Rayleigh numbers. Pirmohammadi and Ghassemi (2009) studied steady laminar natural-convection flow in the presence of a mag-

netic field in a tilted enclosure heated from below and cooled from top and filled with liquid gallium. They found that for a given inclination angle, as the value of Hartmann number increases, the convection heat transfer is reduced. Furthermore they obtained that at $Ra=10^4$, the value of Nusselt number depends strongly on the inclination angle for relatively small values of Hartmann number.

Ece and Buyuk (2006) examined the steady and laminar natural convection flow in the presence of a magnetic field in an inclined rectangular enclosure heated and cooled on its adjacent walls. They found that the magnetic field suppressed the convective flow and the heat transfer rate. They also showed that the orientation and the aspect ratio of the enclosure and the strength and direction of the magnetic field had significant effects on the flow and temperature fields. Sathiyamoorthy and Chamkha (2010) numerically studied natural convection flow of electrically conducting liquid gallium in a square cavity whereas the bottom wall is uniformly heated and the left and right vertical walls are linearly heated while the top wall is kept thermally insulated. They exhibited that the magnetic field with inclined angle has effects on the flow and heat transfer rates in the cavity. Sivasankaran and Ho (2008) studied numerically the effects of temperature dependent properties of the natural convection of water in a cavity under the influence of a magnetic field. They showed that the heat transfer rate was influenced by the direction of the external magnetic field and was decreased with an increase of the magnetic field. Oztop and Abu-Nada (2008) studied the effects of a partial heater on natural convection using different types and concentrations of nanoparticles. They found that heat transfer was strongly related to types and volume fractions of nanoparticles. Abu-Nada (2009); Abu-Nada (2010) and Abu-Nada et al. (2010) studied the effect of the variables properties of nanofluids in natural convection. They related the deterioration in heat transfer of nanofluids in natural convection to the temperature dependence of nanofluid properties. These findings were also supported by other studies [Abu-Nada and Chamkha (2010a); Abu-Nada and Chamkha (2010b)]. Alam et al. (2012) investigated natural convection in a rectangular enclosure due to partial heating and cooling at vertical walls. Fattahi et al. (2012) applied Lattice Boltzmann Method to investigate the natural convection flows utilizing nanofluids in a square cavity. The fluid in the cavity was a water-based nanofluid containing Al_2O_3 or Cu nanoparticles. The results indicated that by increasing solid volume fraction, the average Nusselt number increased for both nanofluids. It was found that the effects of solid volume fraction for Cu were stronger than Al_2O_3 . Kefayati et al. (2011) simulated by the Lattice Boltzmann method the natural convection in enclosures using water/ SiO_2 nanofluid. The results showed that the average Nusselt number increased with volume fraction for the whole range of Rayleigh numbers and aspect ratios. Also the effect of nanoparticles on heat transfer aug-

mented as the enclosure aspect ratio increased. Lai and Yang (2011) performed mathematical modeling to simulate natural convection of Al_2O_3 /water nanofluids in a vertical square enclosure using the Lattice Boltzmann method. The results indicated that the average Nusselt number increased with the increase of Rayleigh number and particle volume concentration. The average Nusselt number with the use of nanofluid was higher than the use of water under the same Rayleigh number. Mahmoudi et al. (2011) presented a numerical study of natural convection cooling of two heat sources vertically attached to horizontal walls of a cavity. The results indicated that the flow field and temperature distributions inside the cavity were strongly dependent on the Rayleigh numbers and the position of the heat sources. The results also indicated that the Nusselt number was an increasing function of the Rayleigh number, the distance between two heat sources, and distance from the wall and the average Nusselt number increased linearly with the increase in the solid volume fraction of nanoparticles. Kefayati et al. (2013) investigated Prandtl number effect on natural convection MHD in an open cavity which has been filled respectively with liquid gallium, air and water by Lattice Boltzmann Method. They exhibited that heat transfer declines with the increment of Hartmann number, while this reduction is marginal for $\text{Ra}=10^3$ by comparison with other Rayleigh numbers. Lattice Boltzmann Method simulation of MHD mixed convection in a lid-driven square cavity with linearly heated wall is investigated by Kefayati et al. (2012). It was demonstrated that the augmentation of Richardson number causes heat transfer to increase, as the heat transfer decreases by the increment of Hartmann number for various Richardson numbers and the directions of the magnetic field. The LBM is an applicable method for simulating fluid flow and heat transfer [Nemati et al. (2010); Mehravaran and Hannani (2011); Pirouz et al. (2011); Mohamad (2007); Succi (2001)]. This method was also applied to simulate the MHD [Martinez et al. (1994)] and, recently, nanofluid [Nemati et al. (2010)] successfully.

The aim of the present study is to assess the ability of Lattice Boltzmann Method (LBM) in solving a nanofluid and a magnetic field simultaneously in the presence of a sinusoidal thermal boundary condition. Moreover, the effects of magnetic field and phase deviations on the heat transfer in the cavity are considered in order to identify the best situation for heat transfer and fluid flow.

2 Mathematical formulation

2.1 Problem statement

A two-dimensional square cavity is considered as shown in Fig. 1. The side walls of the cavity have spatially varying sinusoidal temperature distributions. The horizontal walls are adiabatic. The cavity is filled with water and Al_2O_3 nanoparticles.

The nanofluid is assumed to be Newtonian and incompressible. The flow is considered to be steady, two dimensional and laminar, while the radiation effects are assumed to be negligible. The thermo-physical properties of the base fluid and the nanoparticles are given in Table 1. The density variation in the nanofluid is approximated by the standard Boussinesq model.

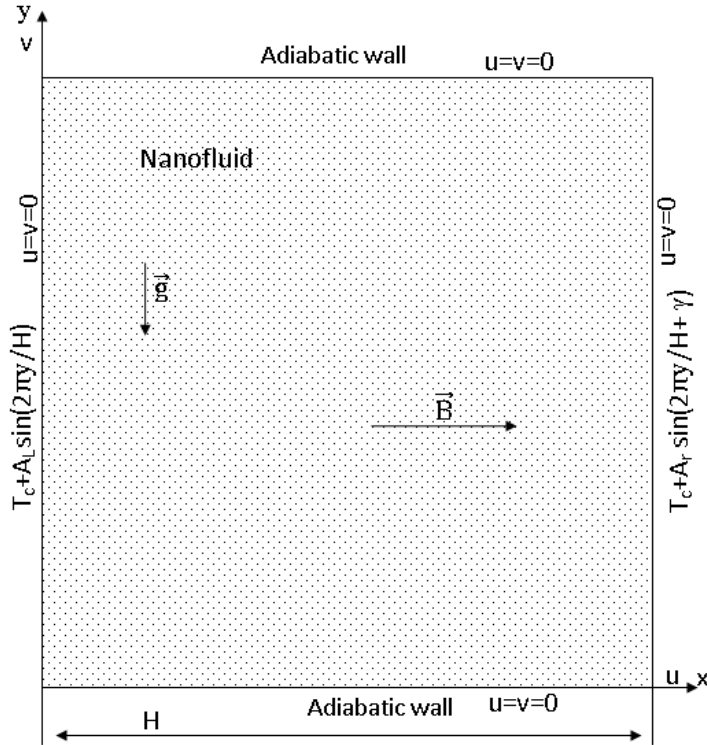


Figure 1: Geometry of the present study with boundary conditions.

Table 1: Thermo-physical properties of water and nanoparticles. [Ghasemi and Aminossadati (2010)]

	ρ (kg/m ³)	C_p (J/kg K)	K (W/mK)	β (K ⁻¹)
Pure water	997.1	4179	0.613	21×10^{-5}
Al₂O₃	3970	765	40	0.85×10^{-5}
Cu	8933	385	400	1.67×10^{-5}
TiO₂	4250	686.2	8.9538	0.9×10^{-5}

The magnetic field (strength B_0) is applied in the horizontal direction. It is assumed that the induced magnetic field produced by the motion of an electrically conducting fluid is negligible compared to the applied magnetic field. Furthermore, it is assumed that the viscous dissipation and Joule heating can be neglected.

Therefore, governing equations are written in dimensional form as:

$$\frac{\partial u}{\partial x} + \frac{\partial v}{\partial y} = 0 \quad (1)$$

$$\rho_{nf} \left(u \frac{\partial u}{\partial x} + v \frac{\partial u}{\partial y} \right) = -\frac{\partial p}{\partial x} + \mu_{nf} \left(\frac{\partial^2 u}{\partial x^2} + \frac{\partial^2 u}{\partial y^2} \right) \quad (2)$$

$$\rho_{nf} \left(u \frac{\partial v}{\partial x} + v \frac{\partial v}{\partial y} \right) = -\frac{\partial p}{\partial y} + \mu_{nf} \left(\frac{\partial^2 v}{\partial x^2} + \frac{\partial^2 v}{\partial y^2} \right) + F_y \quad (3)$$

$$u \frac{\partial T}{\partial x} + v \frac{\partial T}{\partial y} = \alpha_{nf} \left(\frac{\partial^2 T}{\partial x^2} + \frac{\partial^2 T}{\partial y^2} \right) \quad (4)$$

Where F_y is the total body forces at y direction and it is defined as follows:

$$F_y = -\frac{Ha^2 \mu_{nf}}{H^2} v + (\rho\beta)_{nf} g (T - T_m) \quad (5)$$

Where Ha is $Ha = HB_0 \sqrt{\frac{\sigma_{nf}}{\mu_{nf}}}$

The classical models reported in the literature are used to determine the properties of the nanofluid [Xuan and Roetzel (2000)]:

$$\rho_{nf} = (1 - \phi)\rho_f + \phi\rho_p \quad (6)$$

$$(\rho c_p)_{nf} = (1 - \phi)(\rho c_p)_f + \phi(\rho c_p)_p \quad (7)$$

$$(\rho\beta)_{nf} = (1 - \phi)(\rho\beta)_f + \phi(\rho\beta)_p \quad (8)$$

$$\alpha_{nf} = \frac{k_{nf}}{(\rho c_p)_{nf}} \quad (9)$$

In the above equations, ϕ is the solid volume fraction, ρ is the density, σ is the electrical conductivity, α is the thermal diffusivity, c_p is the specific heat at constant pressure and β is the thermal expansion coefficient of the nanofluid, γ is the phase deviation. The effective dynamic viscosity and thermal conductivity of the nanofluid can be modelled by Brinkman (1958); Maxwell (1873):

$$\mu_{nf} = \frac{\mu_f}{(1 - \phi)^{2.5}} \quad (10)$$

$$k_{nf} = k_f \frac{k_p + 2k_f - 2\phi(k_f - k_p)}{k_p + 2k_f + \phi(k_f - k_p)} \quad (11)$$

The governing equations are subject to the following boundary conditions:

$$\begin{aligned} \text{Bottom wall } u = v = 0 \quad \left. \frac{\partial T}{\partial y} \right|_{y=0} &= 0 \\ \text{Top wall } u = v = 0 \quad \left. \frac{\partial T}{\partial y} \right|_{y=H} &= 0 \\ \text{Left wall } u = v = 0 \quad T(0, y) &= T_C + A_l \sin(2\pi y/H) \\ \text{Right wall } u = v = 0 \quad T(H, y) &= T_C + A_r \sin(2\pi \frac{y}{H} + \gamma) \end{aligned} \quad (12)$$

2.2 Simulation of MHD and nanofluid with Lattice Boltzmann Method

For the incompressible non isothermal problems, the Lattice Boltzmann Method (LBM) is based on two distribution functions, f and g , for the flow and temperature fields respectively.

For the flow field:

$$f_i(\mathbf{x} + \mathbf{c}_i \Delta t, t + \Delta t) = f_i(\mathbf{x}, t) - \frac{1}{\tau_v} (f_i(\mathbf{x}, t) - f_i^{eq}(\mathbf{x}, t)) + \Delta t F_i \quad (13)$$

For the temperature field:

$$g_i(\mathbf{x} + \mathbf{c}_i \Delta t, t + \Delta t) = g_i(\mathbf{x}, t) - \frac{1}{\tau_\alpha} (g_i(\mathbf{x}, t) - g_i^{eq}(\mathbf{x}, t)) \quad (14)$$

Where the discrete particle velocity vectors defined by \mathbf{c}_i , Δt denotes lattice time step which is set to unity. τ_v , τ_α are the relaxation time for the flow and temperature fields, respectively. f_i^{eq} , g_i^{eq} are the local equilibrium distribution functions that have an appropriately prescribed functional dependence on the local hydrodynamic properties which are calculated with Eqs. (15) and (16) for flow and temperature fields respectively.

$$f_i^{eq} = \omega_i \rho \left[1 + \frac{3(\mathbf{c}_i \cdot \mathbf{u})}{c^2} + \frac{9(\mathbf{c}_i \cdot \mathbf{u})^2}{2c^4} - \frac{3\mathbf{u}^2}{2c^2} \right] \quad (15)$$

$$g_i^{eq} = \omega'_i T \left[1 + 3 \frac{\mathbf{c}_i \cdot \mathbf{u}}{c^2} \right] \quad (16)$$

\mathbf{u} and ρ are the macroscopic velocity and density, respectively. c is the lattice speed which is equal to $\Delta x/\Delta t$ where Δx is the lattice space similar to the lattice time step Δt which is equal to unity, ω_i is the weighting factor for flow, ω'_i is the weighting

factor for temperature. D2Q9 model for flow and D2Q4 model for temperature are used in this work so that the weighting factors and the discrete particle velocity vectors are different for these two models and they are calculated with Eqs (17-19) as follows:

For D2Q9

$$\omega_0 = \frac{4}{9}, \omega_i = \frac{1}{9} \text{ for } i = 1, 2, 3, 4 \text{ and } \omega_i = \frac{1}{36} \text{ for } i = 5, 6, 7, 8 \quad (17)$$

$$\mathbf{c}_i = \begin{cases} 0 & i = 0 \\ (\cos \cos[(i-1)\pi/2], \sin[(i-1)\pi/2])c & i = 1, 2, 3, 4 \\ \sqrt{2}(\cos[(i-5)\pi/2 + \pi/4], \sin[(i-5)\pi/2 + \pi/4])c & i = 5, 6, 7, 8 \end{cases} \quad (18)$$

For D2Q4

The temperature weighting factor for each direction is equal to $\omega'_i = 1/4$.

$$\mathbf{c}_i = (\cos[(i-1)\pi/2], \sin[(i-1)\pi/2])c \quad i = 1, 2, 3, 4 \quad (19)$$

The kinematic viscosity ν and the thermal diffusivity α are then related to the relaxation time by Eq. (20):

$$\nu = \left[\tau_\nu - \frac{1}{2} \right] c_s^2 \Delta t \quad \alpha = \left[\tau_\alpha - \frac{1}{2} \right] c_s^2 \Delta t \quad (20)$$

Where c_s is the lattice speed of sound which is equal to $c_s = c/\sqrt{3}$. In the simulation of natural convection, the external force term F appearing in Eq. (14) is given by Eq. (21)

$$F_i = \frac{\omega_i}{c_s^2} F \cdot c_i \quad (21)$$

Where $F = F_y$

The macroscopic quantities, \mathbf{u} and T can be calculated by the mentioned variables, with Eq. (22-24).

$$\rho = \sum_i f_i \quad (22)$$

$$\rho \mathbf{u} = \sum_i f_i \mathbf{c}_i \quad (23)$$

$$T = \sum_i g_i \quad (24)$$

2.3 Boundary conditions

The implementation of boundary conditions is very important for the simulation. The distribution functions out of the domain are known from the streaming process. The unknown distribution functions are those toward the domain.

2.3.1 Flow

Bounce-back boundary conditions were applied on all solid boundaries, which mean that incoming boundary populations are equal to out-going populations after the collision.

2.3.2 Temperature

The bounce back boundary condition is used on the adiabatic wall. Temperature at the left and the right walls are known. Since we are using D2Q4, the unknown internal energy distribution functions are evaluated as:

$$\text{Right wall: } g_3 = T(y) - g_1 - g_2 - g_4 \quad (25)$$

$$\text{Left wall: } g_1 = T(y) - g_2 - g_3 - g_4 \quad (26)$$

2.4 Non-dimensional parameters

By fixing Rayleigh number, Prandtl number and Mach number, the viscosity and thermal diffusivity are calculated from the definition of these non dimensional parameters.

$$v_f = N.Ma.c_s \sqrt{\frac{Pr}{Ra}} \quad (27)$$

Where N is number of lattices in y -direction. Rayleigh and Prandtl numbers are defined as $Ra = \frac{g\beta_f H^3 (T_h - T_c)}{v_f \alpha_f}$ and $Pr = \frac{v_f}{\alpha_f}$ respectively. Mach number should be less than $Ma = 0.3$ to insure an incompressible flow. Therefore, in the present study, Mach number was fixed at $Ma = 0.1$. The Hartmann number has a very important role for the control of the effect of the magnetic field $Ha = HB_0 \sqrt{\frac{\sigma_{nf}}{\mu_{nf}}}$. Nusselt number is one of the most important dimensionless parameters in the description of the convective heat transport. The local Nusselt number (Nul and Nur), the average Nusselt number (Nu) and the dimensionless average Nusselt number (Nu^*) are calculated as:

$$Nul = -\frac{k_{nf}}{k_f} \frac{H}{T_h - T_c} \frac{\partial T}{\partial x} \Big|_{x=0} \quad (28)$$

$$Nu_r = -\frac{k_{nf}}{k_f} \frac{H}{T_h - T_c} \left. \frac{\partial T}{\partial x} \right|_{x=H} \quad (29)$$

$$Nu = \frac{1}{H} \int_{\text{heating half}} Nu_r dy + \frac{1}{H} \int_{\text{heating half}} Nu_l dy \quad (30)$$

$$Nu^*(\phi) = \frac{Nu(\phi)}{Nu(\phi=0)} \quad (31)$$

3 Grid testing and validation code:

3.1 Grid testing:

A Lattice Boltzmann Method scheme was used for the numerical simulations. Fig. 2 shows the effect of grid resolution and lattice sizes (20x20), (40x40), (60x60), (80x80) and (100x100) for $Ha=0$ and $\phi = 0$. By calculating the average Nusselt number for $Ra=10^3$ and 10^5 , it was found that a grid size of (100x100) ensures a grid independent solution.

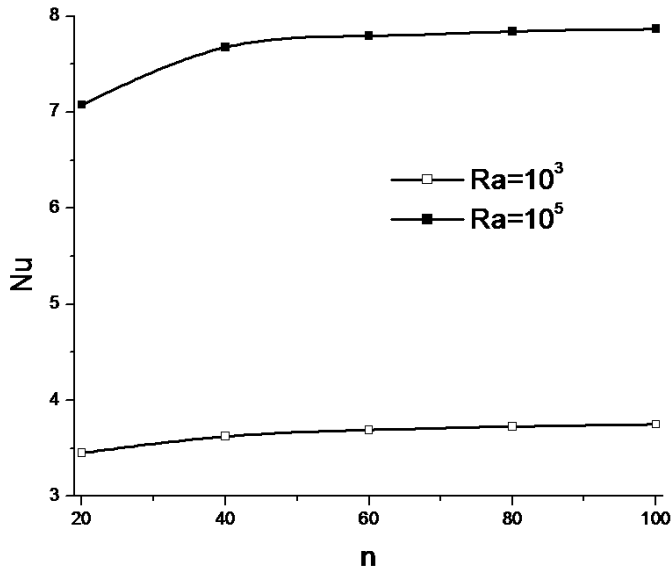
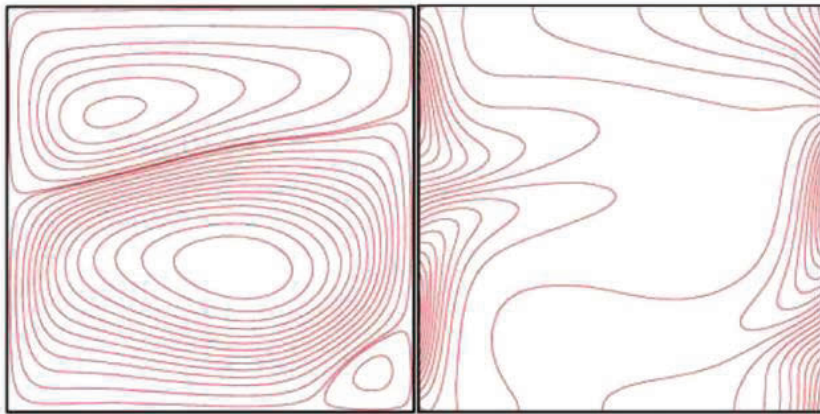
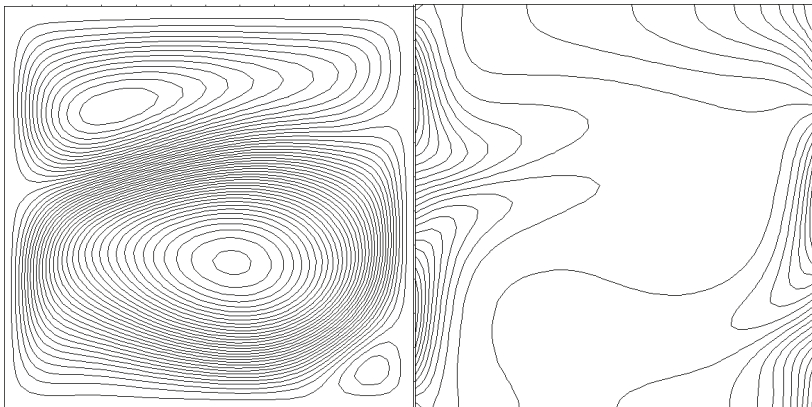


Figure 2: Average Nusselt number for different uniform grids ($\phi = 0$, $\gamma = \pi/2$ and $Ha=0$).



(a)



(b)

Figure 3: Comparison of the streamlines and isotherms for $Ra=10^5$ and $Pr = 0.7$ between (a) numerical results by Deng et al. (2008) and (b) the present result.

3.2 Validation code:

In order to check on the accuracy of the numerical technique employed for the solution of the considered problem, the present numerical code was validated by comparison with the study by Deng and Chang (2008) for the same cavity with sinusoidal boundary conditions for $\gamma = \pi/2$, $Ra=10^5$ and $Pr=0.7$. The results are presented in Fig.3. The results of another validation study comparison with Ghase-mi et al. (2011) are presented in Fig. 4 which shows the dimensionless temperature

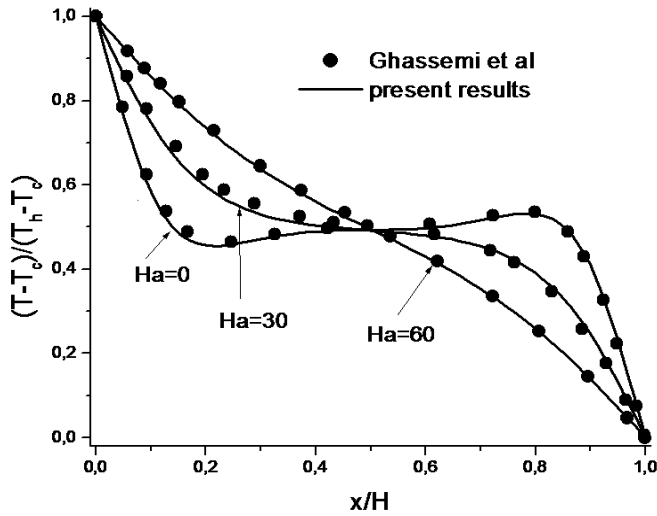


Figure 4: Comparison of the temperature on axial midline between the present results and numerical results by Ghassemi et al., (2011) ($\phi = 0.03, Ra=10^5$).

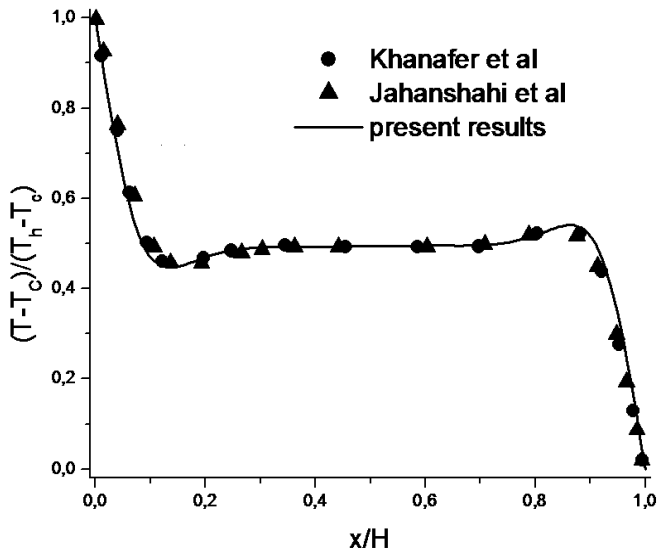


Figure 5: Comparison of the temperature on axial midline between the present results and numerical results by Khanafer et al., (2003) and jahanshahi et al., (2010) ($Pr = 6.2, \phi = 0.1, Gr=10^4$).

along the horizontal axial midline of the enclosure for three values of the Hartmann number, for $Ra=10^5$ and for a solid volume fraction $\phi=0.03$ (excellent agreement is also found). The present code was also validated with the results of Khanafer et al. (2003) and Jahanshahiet al. (2010) for natural convection in an enclosure filled with water/Cu nanofluid for $Ra=6.2 \times 10^5$ and $\phi=0.1$ as shown in Fig.5.

4 Results and discussion:

Fig.6 and 7 illustrate the effect of Hartmann number for different values of the Rayleigh number ($Ra = 10^3, 10^4, 10^5$ and 10^6) and for $\gamma = \pi/2$ on the isotherms and streamlines of nanofluid ($\phi=0.04$) and pure fluid ($\phi=0$). For all Rayleigh number it demonstrates that the effect of nanoparticles on the isotherms decreases with the augmentation of Hartmann number. The thickness of the boundary layer decreases with the rise of Rayleigh number, the opposite effect occurs with the increase of the Hartmann number. Fig.8.a shows the variation of average Nusselt number as function of Hartmann number for different Rayleigh number, the increase of Rayleigh number increases the heat transfer rate, on the contrary, the increase of the Hartmann decreases the heat transfer rate. The streamlines shows that the flow behavior is affected with the change in the Rayleigh number and the Hartmann number. At $Ra = 10^3-10^4$ and in the absence of magnetic field, the flow is characterized by two cells, one above the other, rotating in opposite direction inside the enclosure. The minor cell near the let-top corner is elongated when the Hartmann number is increased to 30 and 60 and when Rayleigh number is increased to 10^5 and 10^6 also a third cell appears near the right-bottom corner. The strength of these cells increases as the Rayleigh number increases and decreases as the Hartmann number increases. For all values of Rayleigh number, the application of the magnetic field has the tendency to slow down the movement of the fluid in the enclosure. The braking effect of the magnetic field is observed from the maximum intensity of circulation $|\psi|_{max}$ (Fig.8.b) presents the variation of the maximum value of the stream function as a function of Hartman number for several values of Rayleigh number for $\phi=0$ and $\gamma = \pi/2$. It is observed that the effect of Hartmann number is opposite to the effect of Rayleigh number. For $Ra = 10^3$ and 10^4 , $|\psi|_{max}$ is constant and small for all values of Hartmann number. The conduction is dominant. For $Ra = 10^5$ and 10^6 , the convection is dominant for low values of Hartmann number, more than the Hartmann number increases convection is more disadvantaged, until reaching the conductive regime.

Fig.9. a and b illustrate the variations of the local Nusselt numbers along the left sidewall and right sidewall at various Rayleigh numbers for $Ha=0$ and 60. For both walls, the curves drawn for the Nusselt numbers against y/H are approximately of sinusoidal shape like the thermal boundary. This indicates that the local heat

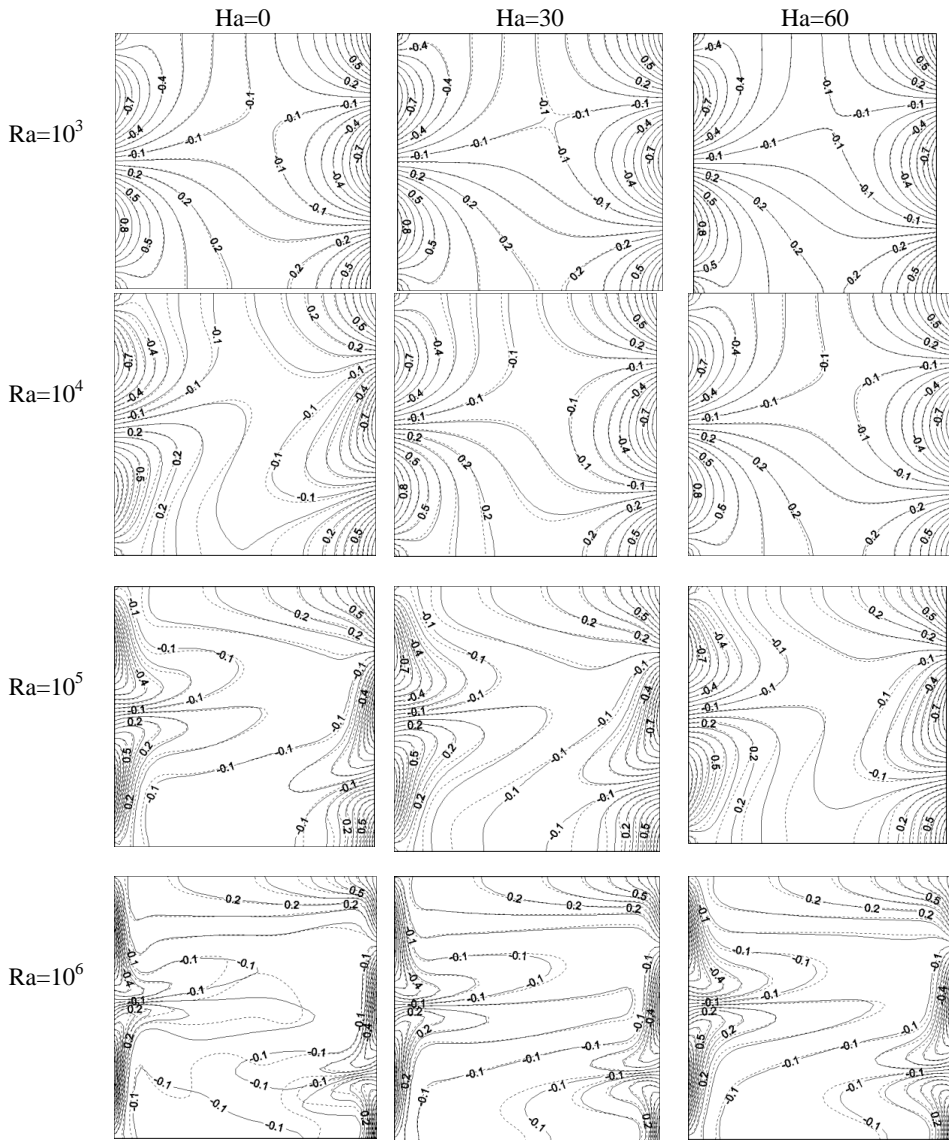


Figure 6: isotherms for different Hartmann and Rayleigh numbers and for $\gamma = \pi/2$, (—) $\phi = 0.04$ and (- - -) $\phi = 0$.

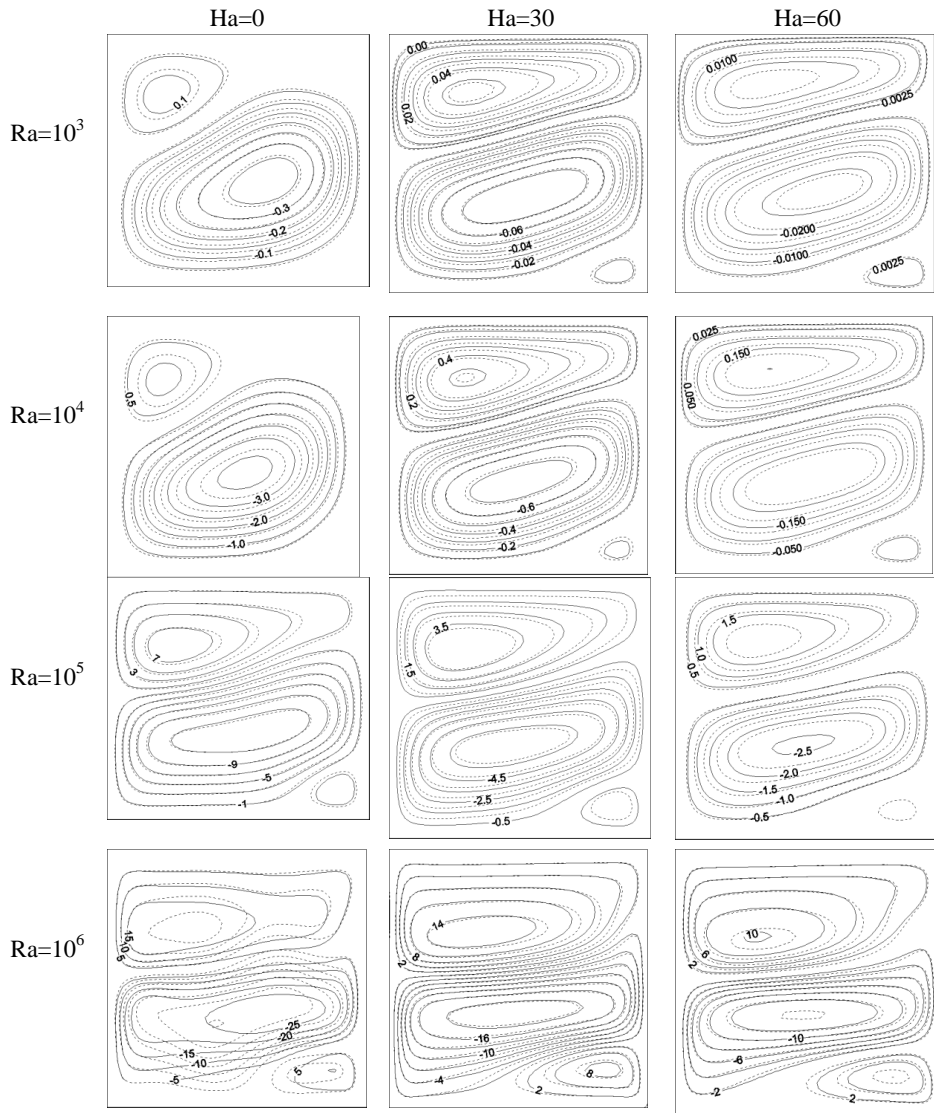


Figure 7: Streamlines for different Hartmann and Rayleigh numbers and for $\gamma = \pi/2$, (—) $\phi = 0.04$ and (- - -) $\phi = 0$.

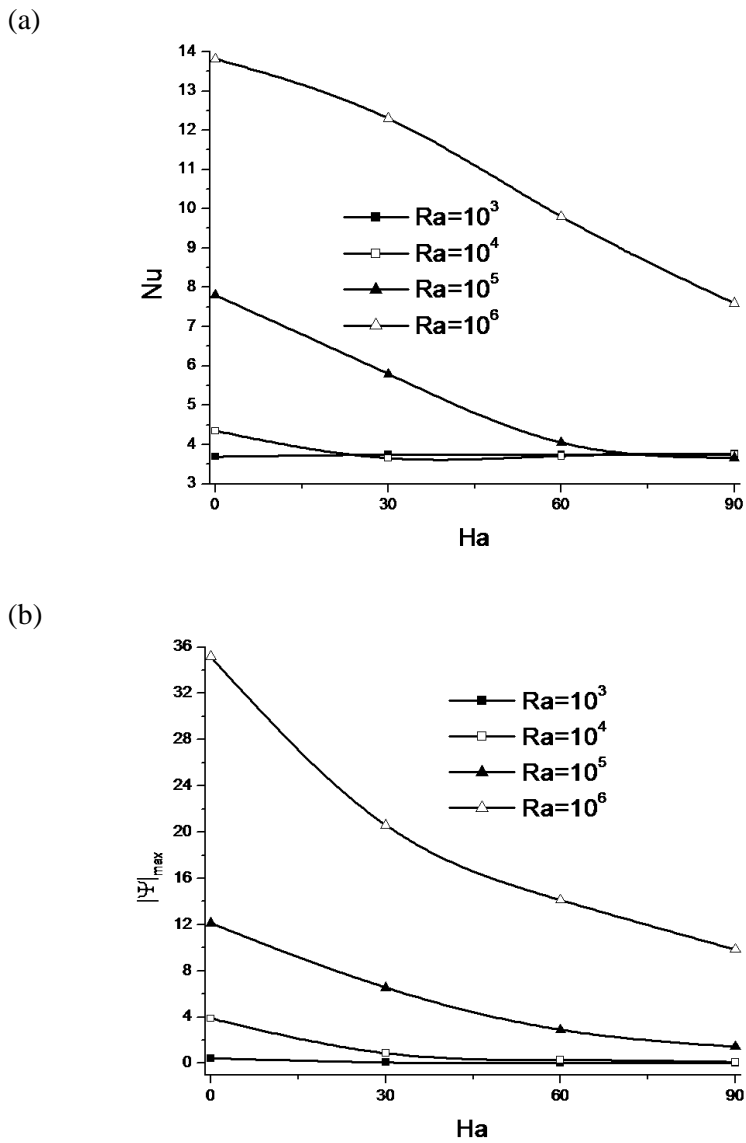
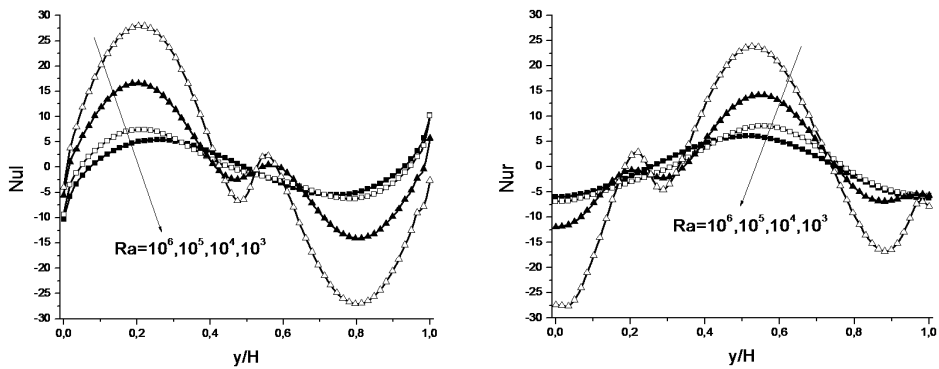
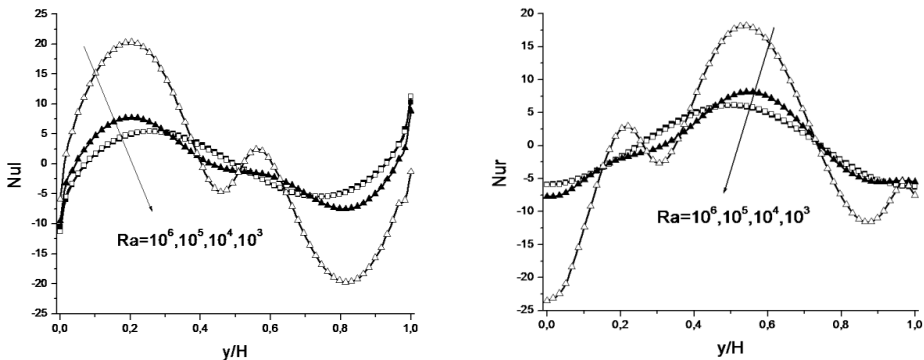


Figure 8: Variation of the maximum of the average Nusselt number (a) and stream function (b) with Hartmann number for different Rayleigh number for $\gamma = \pi/2$ and $\phi = 0$.

transfer is directly affected by the temperature distribution on the surface. In other words, larger heat transfer occurs when the temperature is higher. In the left sidewall, it is obviously understood that the lower half ($0 \leq y/H \leq 0.5$) is the heating half and the upper half ($0.5 \leq y/H \leq 1$) is the cooling half. The variations of the local Nusselt numbers along the left sidewall and the right sidewall are exhibited in Fig.10.a and b for various Hartmann numbers. At $Ra \leq 10^4$ the heat transfer gets no remarkable change on both sidewalls even if the Hartmann number is increased but for $10^4 < Ra \leq 10^6$ it seems that the Nusselt number decreases while the Hartmann number is increased.

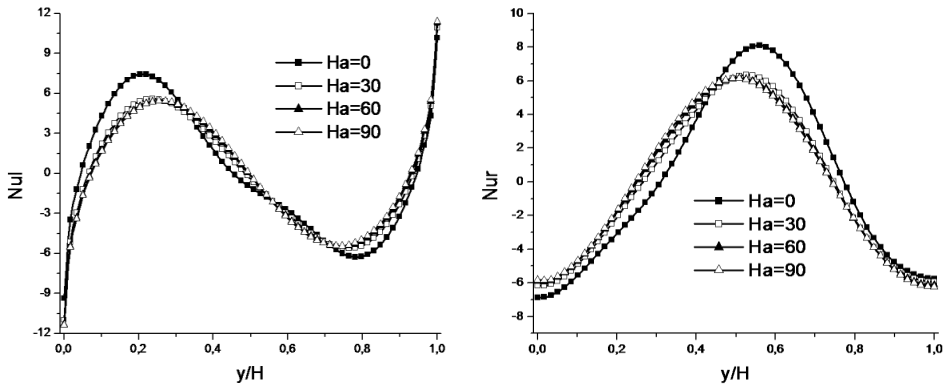


(a)

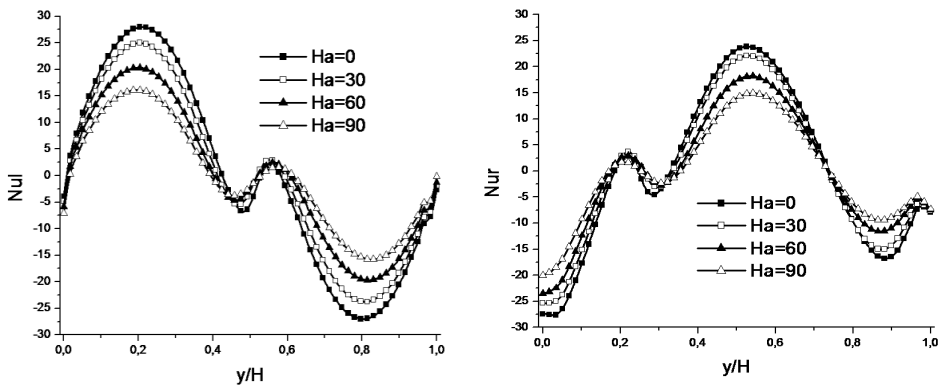


(b)

Figure 9: Variation of the local Nusselt number on the left and the right walls for different Rayleigh number for $Ha=0$ (a) and $Ha=60$ (b) for $\gamma = \pi/2$ and $\phi = 0$.



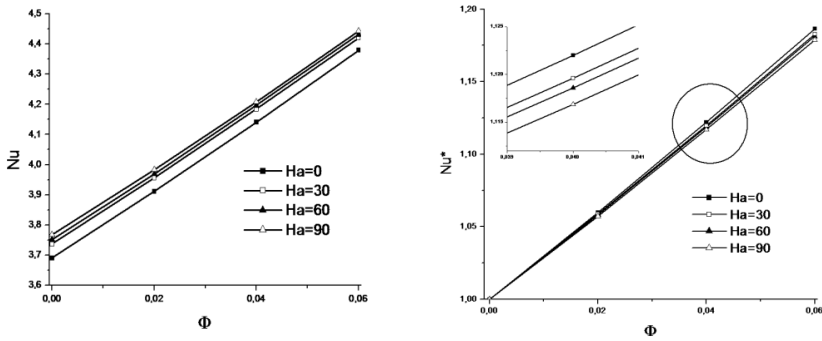
(a)



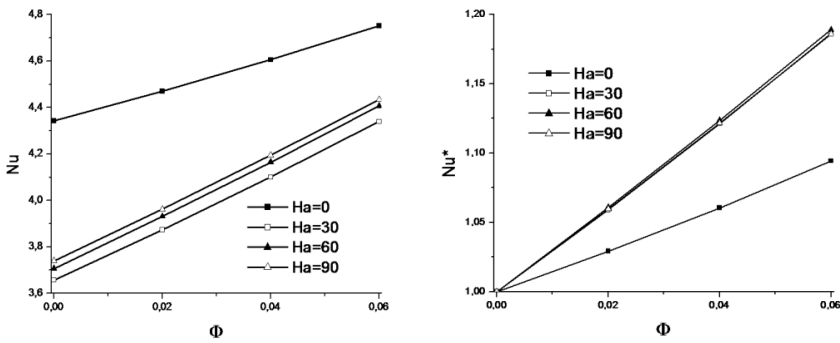
(b)

Figure 10: Variation of the local Nusselt number on the left and the right walls for different Hartmann number for $Ra=10^4$ (a) and $Ra=10^6$ (b) for $\gamma = \pi/2$ and $\phi = 0$.

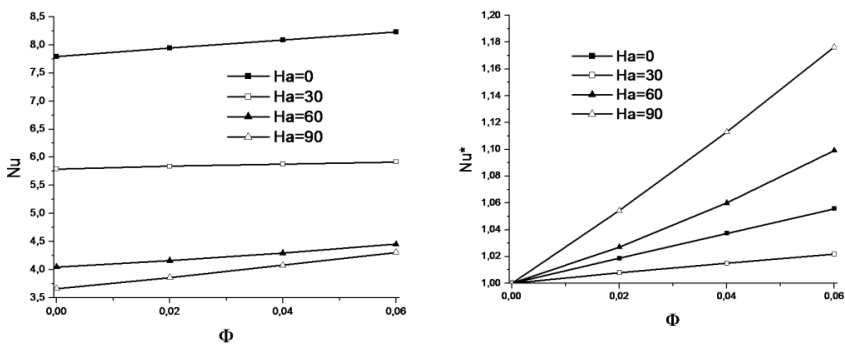
Fig.11 shows comparison of the average Nusselt number and the dimensionless average Nusselt number for various Hartmann and Rayleigh numbers at different volume fractions for $\gamma = \pi/2$. The average Nusselt number demonstrates that heat transfer increases with the enhancement of Hartmann number at $Ra=10^3$. For 10^4 heat transfer declines with the enhancement of Hartmann number from $Ha=0$ to 30 but the average Nusselt number of $Ha=90$ is more than $Ha=60$. Indisputably, the best parameter for showing the effect of the addition of nanoparticles to the



(a)



(b)



(c)

Figure 11: Variation of the average Nusselt number and dimensionless average Nusselt number as function of solid volume fraction for different Hartmann number for $\gamma = \pi/2$, $Ra=10^3$ (a) $Ra=10^4$ (b) and $Ra=10^5$ (c).

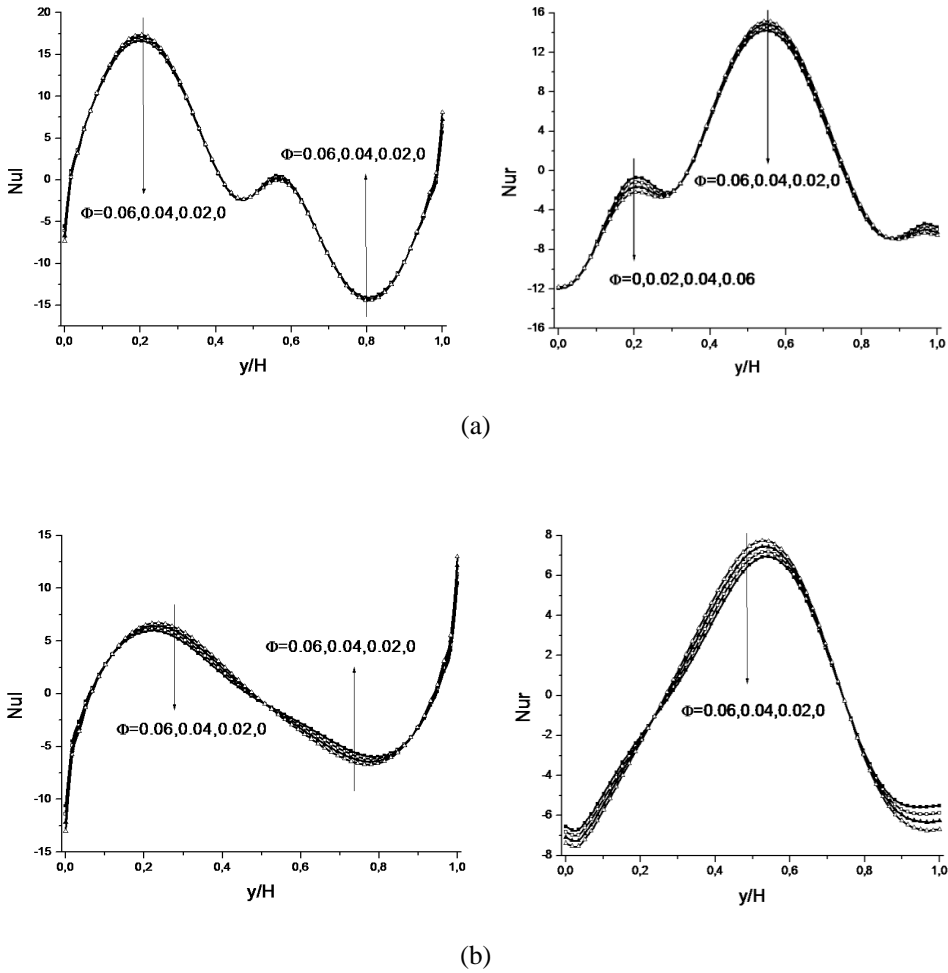


Figure 12: Variation of the local Nusselt number on the left and the right walls for different solid volume fraction at $\gamma = \pi/2$, $Ra=10^5$ for $Ha=0$ (a) and $Ha=90$ (b).

pure fluid is the dimensionless average Nusselt number. At $Ra=10^3$, the best effect of nanoparticles is obtained for $Ha = 0$, by increasing the Hartmann number the effect of nanoparticles decreases. At $Ra=10^4$ the lowest effect of nanoparticles is obtained for $Ha = 0$, for $Ha=30-90$ the nanoparticles have the same tendency to the increase of the solid volume fraction. At $Ra=10^4$ the lowest effect of nanoparticles is obtained for $Ha = 0$, for $Ha=30-90$ the nanoparticles have the same tendency to the increase of the heat transfer. At $Ra=10^5$, the augmentation of Hartmann number play a positive role in the improvement of nanoparticles effect on heat transfer albeit

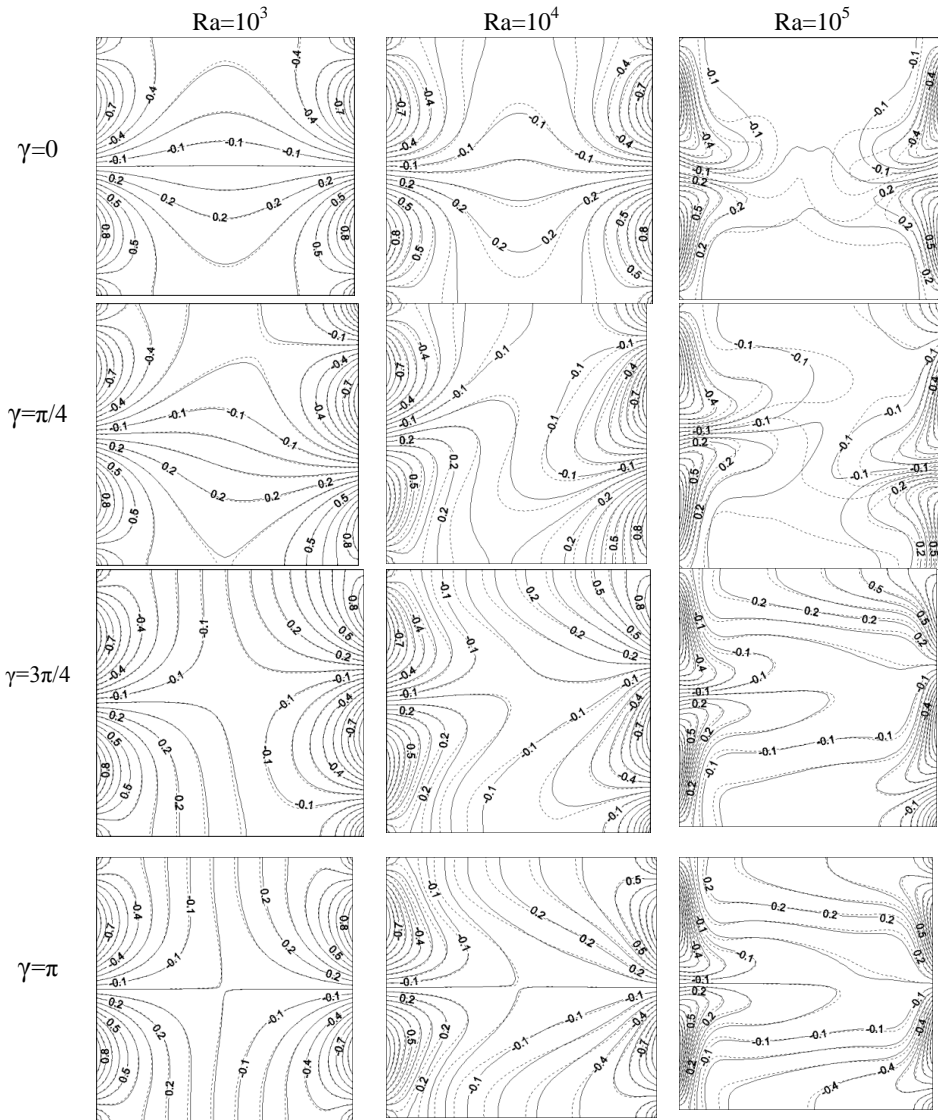


Figure 13: Isotherms for different Rayleigh number and phase deviations for $Ha=0$, (—) $\phi = 0.04$ and (---) $\phi = 0$.

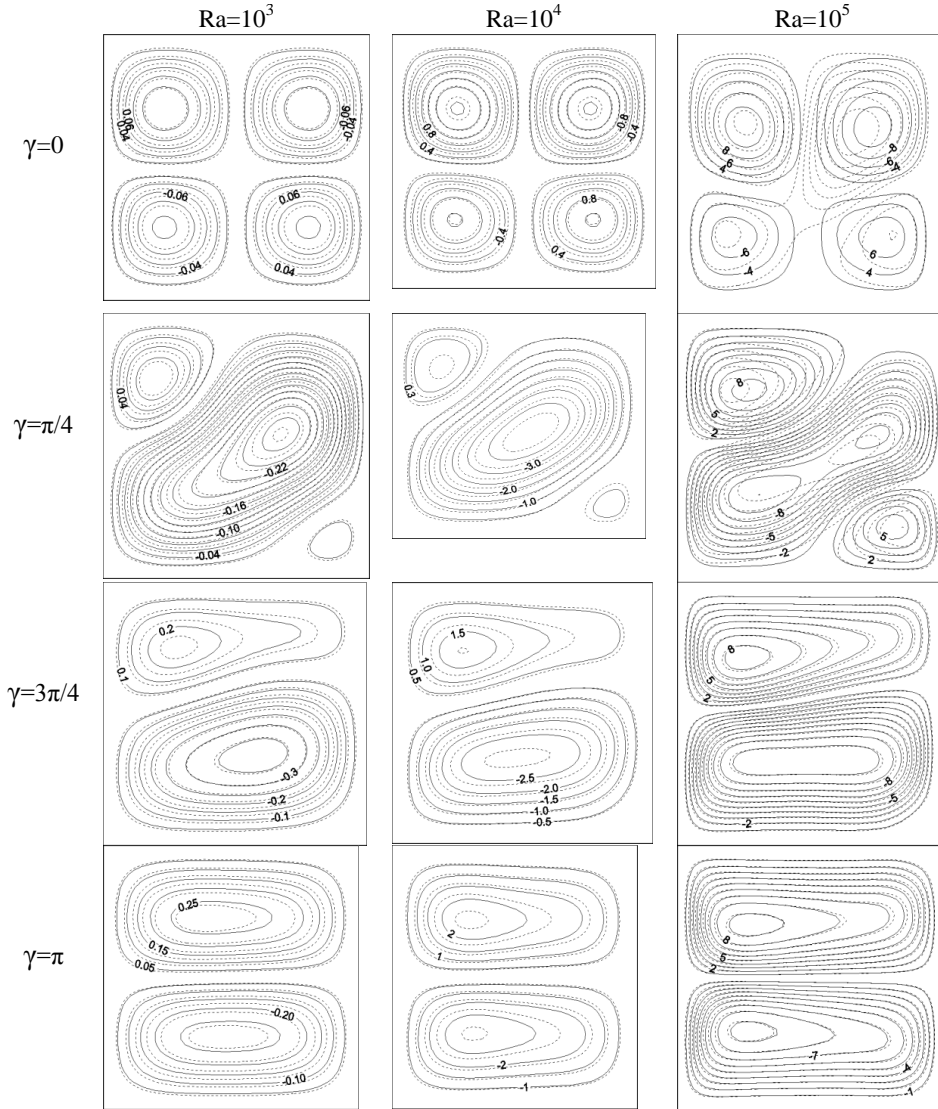


Figure 14: Streamlines for different Rayleigh number and phase deviations for $Ha=0$, (—) $\phi = 0.04$ and (- - -) $\phi = 0$.

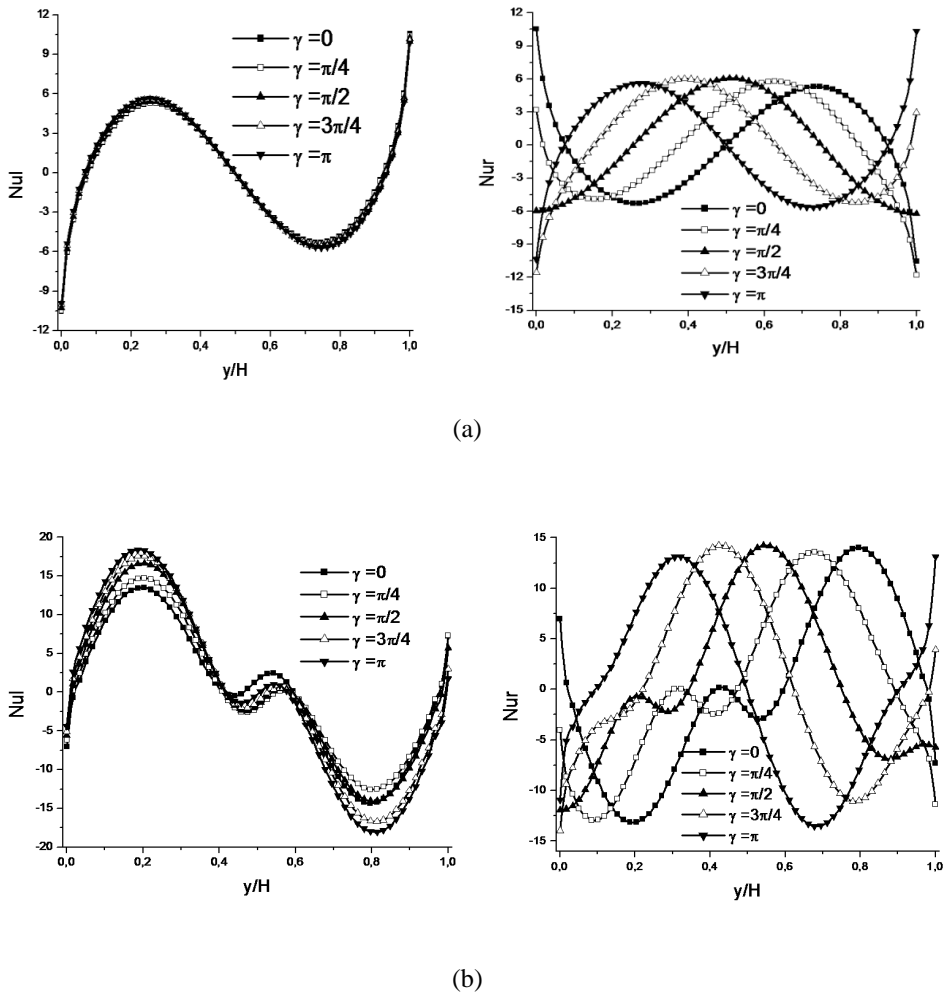
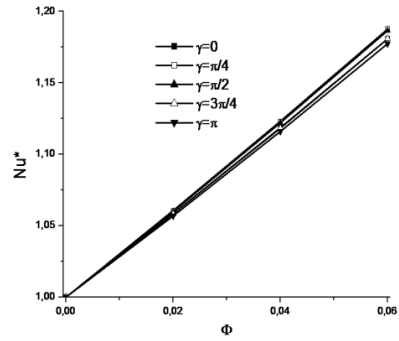
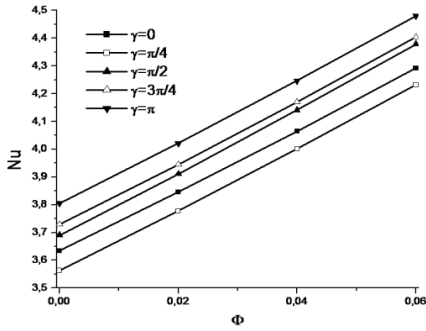


Figure 15: Variation of the local Nusselt number on the left and the right walls for different phase deviations at $Ha=0$ and $\phi=0$ for $Ra=10^3$ (a) and $Ra=10^5$ (b).

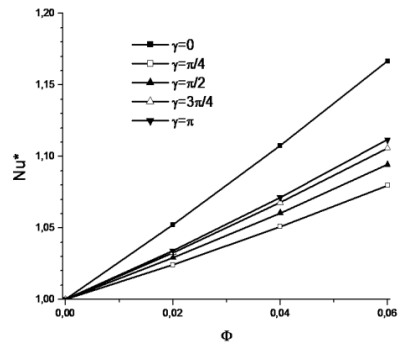
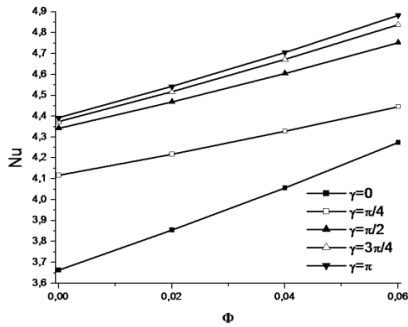
the tendency ceases from $Ha=60$ to 90 .

Fig.12.a and b indicate the local Nusselt number on the right and left sidewalls for various volume fractions at $Ra=10^5$, $\gamma=\pi/2$ and $Ha=0-90$. It is shown that the effect of nanoparticles is more significant for $Ha=90$ which is consistent with Fig.11.

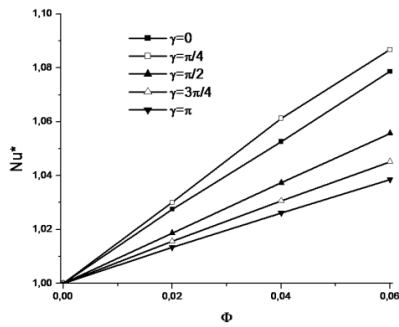
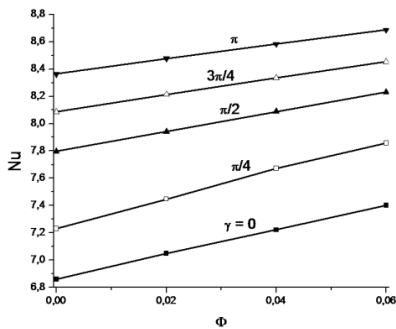
Fig.13 and 14 illustrate the effect of Rayleigh number ($Ra=10^3, 10^4$ and 10^5) for different phase deviation ($\gamma=0, \pi/4, 3\pi/2$ and π) and for $Ha=0$ on the isotherms



(a)



(b)



(c)

Figure 16: Variation of the average Nusselt number and dimensionless average Nusselt number as function of solid volume fraction for different phase deviations for $Ha=0$, $Ra=10^3$ (a) $Ra=10^4$ (b) and $Ra=10^5$ (c).

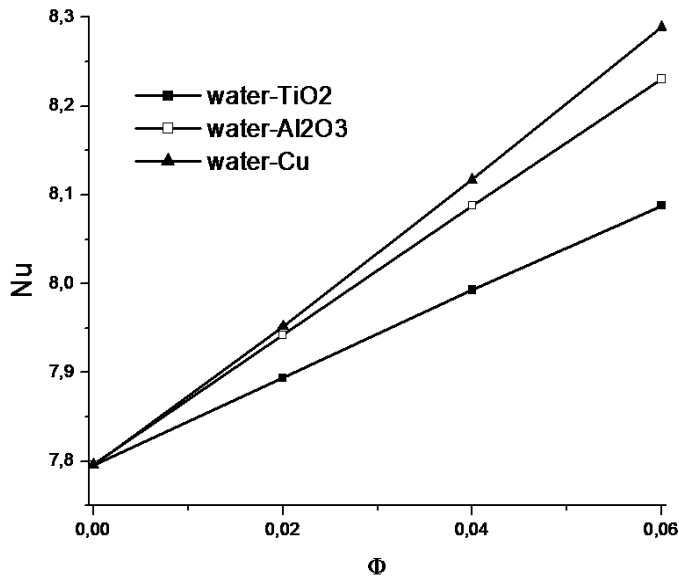


Figure 17: Comparison between different nanofluids at $\gamma = \pi/2$, $Ha = 0$ and $Ra = 10^5$.

and streamlines of nanofluid ($\phi=0.04$) and pure fluid ($\phi=0$). It shown the isotherms along the left sidewall are retained. Hence, the heat transfer on the left sidewall is kept fixed, but that on the right sidewall is varied. At $\gamma = 0$, for $Ra < 10^5$ four cells are formed with approximately symmetries about middle of the cavity, for $Ra = 10^5$ symmetry is broken only for $\phi=0$. As the phase deviation increases up to $\gamma = \pi/4$, a multi-cellular flow structure is formed in the cavity with one large diagonal cell and two smaller corner cells. As the phase deviation increases, the size of the upper left-corner cell is enlarged but the lower right-corner cell disappears. At $\gamma = \pi$, the flow structure is of two identical cells in the enclosure.

Fig.15. a and b show the effect of the phase deviation for $Ra = 10^3$ and 10^5 on the local Nusselt number along the y coordinates of the two vertical sidewalls at $\phi=0$ and $Ha=0$. At $Ra = 10^3$ it is observed that the heat transfer of the left wall is not affected so much on changing the phase deviation, but the heat transfer of the right wall is affected significantly on changing the phase deviation from $\gamma = 0$ to π . The local Nusselt number curves are approximately of sinusoidal shape like the thermal boundary along the vertical walls. This clearly shows that the local heat transfer is directly affected by the temperature distribution on the surface. It is also found that a higher heat transfer occurs where the temperature is higher. At $Ra = 10^5$ the local Nusselt number along the right side wall is greatly affected by changing the phase deviation. It is also found that the local Nusselt number is increased as the

Rayleigh number increases.

Fig.16 shows the effects of volume fractions and phase deviations for various Rayleigh numbers on the average Nusselt number and the dimensionless average Nusselt number. For all Rayleigh number and phase deviations the heat transfer increases with the rise of volume fraction. For $Ra=10^3$ heat transfer decreases from $\gamma=0$ to $\pi/4$ and increases from $\gamma=\pi/2$ to π . Moreover, the dimensionless average Nusselt number has the same trend in different phase deviations. The nanofluids have effects very similar for all phase deviations. At $Ra=10^4$ and 10^5 heat transfer increases with the rise of phase deviations, the most heat transfer was obtained in $\gamma=\pi$. the best effect of nanoparticles for $Ra=10^4$ and 10^5 is obtained in $\gamma=0$ and $\pi/4$ respectively.

Fig.17 shows the effect of nature of nanoparticles on heat transfer. Three nanoparticles are compared at $Ra=10^5$, $Ha=0$ and $\gamma=\pi/2$. The heat transfer depends strongly on the nano thermal conductivity, so water-Cu nanofluid enhances the heat transfer compared with water- Al_2O_3 and water- TiO_2 . **Table 1** shows the proportionally to the solid volume fraction.

5 Conclusions:

In this paper the effect of a magnetic field on a nanofluid flow in a cavity with a sinusoidal thermal boundary condition has been analyzed in the framework of a Lattice Boltzmann Method. The main conclusions can be summarized as follows:

- The good agreement with earlier numerical results demonstrates that the Lattice Boltzmann Method is an appropriate technique for these problems.
- for $\gamma=\pi/2$, heat transfer and fluid flow decrease with an increase in the Hartmann number while they increase with an increase in the Rayleigh number.
- At $\gamma=\pi/2$, the growth of nanoparticles volume fraction improves heat transfer for Hartmann number from $Ha=0$ to 90 and for Rayleigh number from $Ra=10^3$ to 10^5 . For $Ra=10^5$ the most evident effect of nanoparticles is obtained for $Ha=90$.
- For all phase deviations the growth of nanoparticles volume fraction improves heat transfer. At $Ra=10^5$ and $Ha=0$ the heat transfer rate increases with the rise of phase deviations, the most evident effect of nanoparticles is obtained for $\gamma=\pi/4$.

References

Abu-Nada, E. (2009): Effects of variable viscosity and thermal conductivity of Al_2O_3 -water nanofluid on heat transfer enhancement in natural convection. *International Journal of Heat and Fluid Flow*, vol. 30, pp. 679–690.

Abu-Nada, E. (2010): Effects of variable viscosity and thermal conductivity of CuO -water nanofluid on heat transfer enhancement in natural convection: mathematical model and simulation. *ASME Journal of Heat Transfer*, vol. 132, pp. 052401.

Abu-Nada, E.; Chamkha, A. (2010a): Effect of nanofluid variable properties on natural convection in enclosures filled with a CuO -EG-water nanofluid. *International Journal of Thermal Sciences*, vol. 49, pp. 2339–2352.

Abu-Nada, E.; Chamkha, A. (2010b): Mixed convection flow in a lid-driven inclined square enclosure filled with a nanofluid. *European Journal of Mechanics B Fluids*, vol. 29, pp. 472–482.

Abu-Nada, E.; Masoud, Z.; Oztop, H.; Campo, A. (2010): Effect of nanofluid variable properties on natural convection in enclosures. *International Journal of Thermal Sciences*, vol. 49, pp. 479–491.

Al-Ajmi, R.; Mosaad, M., (2012): Heat Exchange between Film Condensation and Porous Natural Convection across a Vertical Wall. *Fluid Dyn. Mater. Process.*, vol. 8, no. 1, pp. 51-68

Alam, P.; Kumar, A.; Kapoor, S.; Ansari, S. R. (2012): Numerical investigation of natural convection in a rectangular enclosure due to partial heating and cooling at vertical walls. *Communications in Nonlinear Science and Numerical Simulation*, vol. 17, pp. 2403–2414.

Alchaar, S.; Vasseur, P.; Bilgen, E. (1995): Natural convection heat transfer in a rectangular enclosure with a transverse magnetic field. *Journal of Heat Transfer*, vol. 117, pp. 668-673.

Arid, A.; Kousksou, T.; Jegadheeswaran, S.; Jamil, A.; Zeraouli, Y. (2012): Numerical Simulation of Ice Melting Near the Density Inversion Point under Periodic Thermal Boundary Conditions. *Fluid Dyn. Mater. Process*, vol. 8, no.3, pp. 257-276.

Brinkman, H. C. (1952): The viscosity of concentrated suspensions and solution. *The Journal of Chemical Physics*, vol. 20, pp. 571-581.

Choukairy, K.; Bennacer, R. (2012): Numerical and Analytical Analysis of the Thermosolutal Convection in an Heterogeneous Porous Cavity. *Fluid Dyn. Mater. Process*, vol. 8, no.2, pp. 155-172.

Deng, Q. H.; Chang, J. (2008): Natural convection in a rectangular enclosure with

sinusoidal temperature distributions on both sidewalls. *Numer. Heat Transfer A*, vol. 54, pp. 507–524.

Dihmani, N.; Amraqui, S.; Mezrhab, A.; Laraqi, N. (2012): Numerical Modelling of Rib Width and Surface Radiation Effect on Natural Convection in a Vertical Vented and Divided Channel. *Fluid Dyn. Mater. Process*, vol. 8, no.3, pp. 311-322

Ece, M. C.; Buyuk, E. (2006): Natural-convection flow under a magnetic field in an inclined rectangular enclosure heated and cooled on adjacent walls. *Fluid Dynamics Research*, vol. 38, pp. 564-590.

Fattahi, E.; Farhadi, M.; Sedighi, K.; Nemati, H. (2012): Lattice Boltzmann simulation of natural convection heat transfer in nanofluids. *International Journal of Thermal Sciences*, vol. 52, pp. 91-101.

Garandet, J. P.; Alboussiere, T.; Moreau, R. (1992): Buoyancy driven convection in a rectangular enclosure with a transverse magnetic field. *International Journal of Heat and Mass Transfer*, vol. 35, pp. 741-748.

Ghasemi, B.; Aminossadati, S. M. (2010): Periodic natural convection in a nanofluid-filled enclosure with oscillating heat flux”, *International Journal of Thermal Sciences*, vol. 49, pp. 1-9.

Ghasemi, B.; Aminossadati, S. M.; Raisi, A. (2011): Magnetic field effect on natural convection in a nanofluid-filled square enclosure. *International Journal of Thermal Sciences*, vol. 50, pp. 1748-1756.

Hamimid, S.; Guellal, M.; Amroune, A.; Zeraibi, N. (2012): Effect of a Porous Layer on the Flow Structure and Heat Transfer in a Square Cavity. *Fluid Dyn. Mater. Process*, vol. 8, no. 1, pp. 69-90.

Haslavsky, V.; Miroshnichenko, E.; Kit, E.; Gelfgat, A. Yu. (2013): Comparison and a Possible Source of Disagreement between Experimental and Numerical Results in a Czochralski Model. *Fluid Dyn. Mater. Process*, vol. 9, no.3, pp. 209-234.

Jahanshahi, M.; Hosseinizadeh, S. F.; Alipanah, M.; Deghani, A.; Vakilinejad, G. R. (2010): Numerical simulation of free convection based on experimental measured conductivity in a square cavity using Water/SiO₂ nanofluid. *International Communications in Heat and Mass Transfer*, vol. 37, pp. 687–694.

Kahveci, K. (2010): Buoyancy driven heat transfer of nanofluids in a tilted enclosure. *Journal of Heat Transfer*, vol. 132, pp. 062501.

Kamath, P. M.; Balaji, C.; Venkateshan, S. P. (2013): Heat transfer studies in a vertical channel filled with porous medium. *Fluid Dyn. Mater. Process*, vol. 9, no.2, pp. 109-124.

- Kefayati, G. H. R.; Hosseinizaeh, S. F.; Gorji, M.; Sajjadi, H.** (2011): Lattice Boltzmann simulation of natural convection in tall enclosures using water/SiO₂ nanofluid. *International Communications in Heat and Mass Transfer*, vol. 38, pp. 798-805.
- Kefayati, G. H. R.; Gorji, M.; Ganji, D. D.; Sajjadi, H.** (2013): Investigation of Prandtl number effect on natural convection MHD in an open cavity by Lattice Boltzmann Method. *Engineering Computations*, vol. 30, pp. 97-116.
- Kefayati, G. H. R.; Gorji, M.; Sajjadi, H.; Ganji, D. D.** (2012): Lattice Boltzmann simulation of MHD mixed convection in a lid-driven square cavity with linearly heated wall. *Scientia Iranica*, vol. 19, pp. 1053–1065.
- Khanafar, K.; Vafai, K.; Lightstone, M.** (2003): Buoyancy-driven heat transfer enhancement in a two-dimensional enclosure utilizing nanofluids. *International Journal of Heat and Mass Transfer*, vol. 46, pp. 3639-3653.
- Lai, F.; Yang, Y.** (2011): Lattice Boltzmann simulation of natural convection heat transfer of Al₂O₃/water nanofluids in a square enclosure. *International Journal of Thermal Sciences*, vol. 50, pp. 1930-1941.
- Mahmoudi, A. H.; Shahi, M.; Shahedin, A. M.; Hemati, N.** (2011): Numerical modeling of natural convection in an open cavity with two vertical thin heat sources subjected to a nanofluid. *International Communications in Heat and Mass Transfer*, vol. 38, pp. 110-118.
- Mahrouche, O.; Najam, M.; El Alami, M.; Faraji, M.** (2013): Mixed Convection Investigation in an Opened Partitioned Heated Cavity. *Fluid Dyn. Mater. Process*, vol. 9, no.3, pp. 235-250.
- Maougal, A.; Bessaïh, R.** (2013): Heat Transfer and Entropy Analysis for Mixed Convection in Discretely Heated Porous Square Cavity. *Fluid Dyn. Mater. Process*, vol. 9, no.1, pp. 35-58
- Martinez, D.; Chen, S.; Matthaeus, W. H.** (1994): Lattice Boltzmann magneto hydrodynamics. *Physics of Plasmas*, vol. 1, pp. 1850–1867.
- Maxwell, J. C.** (1873): A Treatise on Electricity and Magnetism. vol. II, *Oxford University Press*, Cambridge, UK, pp. 54.
- Mehravaran, M.; Hannani, S. K.** (2011): Simulation of buoyant bubble motion in viscous flows employing lattice Boltzmann and level set methods. *Scientia Iranica*, vol. 18, pp. 231–240.
- Mohamad, A. A.** (2007): Applied Lattice Boltzmann Method for transport phenomena, momentum. *Heat and mass transfer*, Sure, Calgary, 2007.
- Moreau, M.** (1990): Magnetohydrodynamics. *Kluwer Academic Publishers*, The Netherlands.

- Moufekkik, F.; Moussaoui, M. A.; Mezrhab, A.; Naji, H.; Bouzidi, M.** (2012): Numerical Study of Double Diffusive Convection in presence of Radiating Gas in a Square Cavity. *Fluid Dyn. Mater. Process*, vol. 8, no.2, pp. 129-154
- Nemati, H.; Farhadi, M.; Sedighi, K.; Fattahi, E.; Darzi, A. A. R.** (2010a): Lattice Boltzmann simulation of nanofluid in lid-driven cavity. *International Communications in Heat and Mass Transfer*, vol. 37, pp. 1528–1534.
- Nemati, H.; Farhadi, M.; Sedighi, K.; Pirouz, M. M.; Fattahi, E.** (2010b): Numerical simulation of fluid flow around two rotating side by side circular cylinders by Lattice Boltzmann method. *International Journal of Computational Fluid Dynamics*, vol. 24, pp. 83–94.
- Ostrach, S.** (1988): Natural convection in enclosures. *Journal of Heat Transfer*, vol. 110, pp. 1175-1190.
- Ozoe, H.; Okada, K.** (1989): The effect of the direction of the external magnetic field on the three dimensional natural convection in a cubical enclosure. *International Journal of Heat and Mass Transfer*, vol. 32, pp. 1939-1954.
- Oztop, H. F.; Abu-Nada, E.** (2008): Numerical study of natural convection in partially heated rectangular enclosure filled with nanofluids. *International Journal of Heat and Fluid Flow*, vol. 29, pp. 1326–1336.
- Pirmohammadi, M.; Ghassemi, M.** (2009): Effect of magnetic field on convection heat transfer inside a tilted square enclosure. *International Communications in Heat and Mass Transfer*, vol. 36, pp. 776-780.
- Pirouz, M. M.; Farhadi, M.; Sedighi, K.; Nemati, H.; Fattahi, E.** (2011): Lattice Boltzmann simulation of conjugate heat transfer in a rectangular channel with wall-mounted obstacles. *Scientia Iranica, Transaction B: Mechanical Engineering*, vol. 18, pp. 213–221.
- Putra, N.; Roetzel, W.; Das, S. K.** (2003): Natural convection of nano-fluids. *Heat and Mass Transfer*, vol. 39, pp. 775-784.
- Rana, G. C.; Thakur, R. C.** (2013): Effect of Suspended Particles on the Onset of Thermal Convection in Compressible Viscoelastic Fluid in a Darcy-Brinkman Porous Medium. *Fluid Dyn. Mater. Process*, vol. 9, no.3, pp. 251-266
- Rtibi, A.; Hasnaoui, M.; Amahmid, A.** (2013): Soret driven thermosolutal convection in an inclined porous layer: search of optimum conditions of separation and validity of the boundary layer theory. *Fluid Dyn. Mater. Process*, vol. 9, no.2, pp. 181-208
- Rudraiah, N.; Barron, R. M.; Venkatachalappa, M.; Subbaraya, C. K.** (1995): Effect of a magnetic field on free convection in a rectangular enclosure. *International Journal of Engineering Science*, vol. 33, pp. 1075-1084.

Sathiyamoorthy, M.; Chamkha, A. (2010): Effect of magnetic field on natural convection flow in a liquid gallium filled square cavity for linearly heated side wall(s). *International Journal of Thermal Sciences*, vol. 49, pp. 1856-1865.

Shemirani, M. M.; Saghir, M. Z. (2013): An Alternative Approach to Minimize the Convection in Growing a Large Diameter Single Bulk Crystal of Si0:25Ge0:75 Alloy in a Vertical Bridgman Furnace. *Fluid Dyn. Mater. Process.*, vol. 9, no.1, pp. 11-22.

Sivasankaran, S.; Ho, C. J. (2008): Effect of temperature dependent properties on MHD convection of water near its density maximum in a square cavity. *International Journal of Thermal Sciences*, vol. 47, pp. 1184-1194.

Succi, S. (2001): The lattice Boltzmann equation for fluid dynamics and beyond. *Clarendon Press*, Oxford, London.

Venkatachalappa, M.; Subbaraya, C. K. (1993): Natural convection in a rectangular enclosure in the presence of a magnetic field with uniform heat flux from the side walls. *Acta Mechanica*, vol. 96, pp. 13-26.

Wen, D.; Ding, Y. (2005): Formulation of nanofluids for natural convective heat transfer applications. *International Journal of Heat and Fluid Flow*, vol. 26, pp. 855–864.

Xuan, Y.; Roetzel, W. (2000): Conceptions for heat transfer correlation of nanofluids. *International Journal of Heat and Mass Transfer*, vol. 43, pp. 3701-3707.